

# Adhesive Layer Modeling in Concrete Beam Strengthened with FRP in an EFG Framework

Mojtaba Haghgoo<sup>1</sup>, Arash Bahar<sup>1\*</sup>

<sup>1</sup> Department of Civil Engineering, Faculty of Civil Engineering, University of Guilan, Rasht Khalij, Fars Highway, Gilan 41996, Iran

\* Corresponding author, e-mail: [bahar@guilan.ac.ir](mailto:bahar@guilan.ac.ir)

Received: 06 December 2021, Accepted: 19 March 2022, Published online: 11 April 2022

## Abstract

The main challenging issue in concrete beam strengthening with FRP plates is the insurance of their joint performance. As been reported, the external load is mainly the primary reason for plate separation. The applied force corresponding to the moment of failure is called the debonding load. This load is of great importance. Besides, the determination of shear stress in the adhesive layer and tensile strain of the FRP plate is of the topics raised in empirical research. This study recommends using numerical methods to avoid the high cost of empirical studies. Here, failure concepts of the cohesive element are utilized. Horizontal and vertical springs are used to represent the properties of this element in which springs' stiffness deputizes cohesive element characteristics and can be adjusted in three linear, nonlinear, and zero-stiffness steps. Springs' stiffness is related to point displacements. So in an element-free Galerkin (EFG) method formulation, a set of springs, beam, and FRP is used to determine these displacements. Using these estimated nodes' displacement values and utilizing springs' stiffness, the unknown parameters included debonding load, glue shear stress, and the tensile strain produced in the FRP plate can be determined. Whole calculations are coded in Matlab software. The results have been compared with the experimental outcomes of Kim and her colleagues' work. These results indicate glue performance can be investigated through spring modeling based on the cohesive element in an EFG framework with adequate accuracy. So, the significant parts of an experimental setup can be avoided.

## Keywords

debonding load, shear stress, cohesive element, Galerkin method, FRP plate, nonlinear spring

## 1 Introduction

One of the critical issues in construction engineering is strengthening the damaged members. Various studies need to be executed to ensure the proper performance of a specific reinforcement technique, which causes immense costs. One of the structural strengthening methods in concrete buildings is to utilize the FRP plate, which has been widely used in recent years. Some advantages of using an FRP plate are increased bending strength, reduced concrete beam cracking, and decreased created crack width [1–4]. Arrangement and installation modes of FRP plates have various types. They are usually fitted in the tension region of the beam, u-shaped jacket, strengthening toward beam height and as longitudinal rebar [2, 3, 5–8]. One of the most recent studies is the article by Khalil Ibrahim and Movahedi Rad, in which a non-prismatic concrete beam with an FRP sheet is reinforced diagonally. The FRP sheet has strengthened concrete in terms of shear strength [9].

FRP materials used in conducted studies were usually carbon, glass, hybrid, or aramid [10, 11]. One of the fundamental issues of using the FRP plate is the correct recognition of the behavior and performance of the adhesive layer, and the function of the glue used between the plate and beam needs to be assured. For this reason, the glue stress needs to be determined so the best kind of glue can be selected. In this regard, limited analytical studies have been carried out based on the bending theory with a simple beam to determine the shear stress and the effects of FRP plate thickness and the adhesive layer. Experimental tests have been used to observe the accuracy level of analytical results [12–14]. The main goal of the present study is to reduce experimental costs, increase accuracy and confidence in the results of superseded analytical studies and eliminate the limits associated with boundary conditions and beams geometry.

Concrete beams strengthened with FRP plate can experience different failure modes. Several failure mechanisms have been identified regarding the connection between the plate and the concrete beam. If the glue does not have a problem until the debonding load is applied and no separation occurs in the interface, the beam failure happens in one of the modes; compressive crushing of the concrete, FRP plate rupture, or beam shear failure [2, 15–18]. The bending strength relations in the code of practice are proposed based on the coupling behavior of the concrete beam and FRP plate with no debonding [19, 20]. If the interacting performance is not maintained, according to Fig. 1, the failure will be in the form of debonding in the interface. This mode is the most common failure reported by numerous researchers. It can occur due to excessive stresses applied to the glue or implementation problems such as improper adhesion or non-uniform distribution of the glue along the plate length. As the design codes suppose no debonding assumptions, this type of failure is critical [20–22].

To determine stresses applied to glue, also investigate its debonding behavior, the failure concept in the cohesive element can be used. This concept was suggested by Dugdale and Barenblatt [23, 24]. A cohesive element has the potential to take into account both the linear and non-linear behavior of the glue. For stress calculation, the relative displacement in the contact surface is needed. So, in the first stage, the deformation of the adhesive layer must be determined [25]. One of the hypotheses for simplifying modeling also reducing the equations is the deformation of the beam, and the relative deformation of the adhesive layer in the third dimension assumes ignorable.

During applying the load, the deformation in the surface of the adhesive stuck to the FRP increases more than the adhesive attached to the concrete side. In the early stages of loading, this deformation is linearly elastic. This study is intended to replace the adhesive layer with a set of springs to handle this elastic behavior. As the load increases, the deformation of the adhesive layers enters softening (nonlinear) phase, which is called damage development. To equate this behavior, the stiffness of the spring assembly is also assumed to be variable. As the load increases,

the spring's stiffness decreases, and the adhesive deformation increases until, at a specific point, the spring's stiffness becomes zero, and separation occurs. Therefore, the main idea of this research is the concept of simulating the behavior of the adhesive layer with a set of horizontal and vertical springs. The stiffness of springs can change in three; linear (elastic), nonlinear (softening or damage development), and zero-stiffness (zero stress, debonding) modes.

The Element Free Galerkin (EFG) method is a numerical technique for measuring nodes displacement. It uses moving least squares (MLS) functions to determine displacement field and construct shape functions.

The EFG method has quick convergence capability, increasing the continuity and derivative orders to the desired value, and is an excellent choice for simulating nonlinear behavior and discontinuities [26, 27].

Based on the defined problem, the stress values in the beam have been computed in a numerical framework. The results show the concrete does not reach the rupture stress before separation occurs in the FRP sheet. So, the effect of rebars has been omitted. If the length of the beam is greater, the concrete might crack early, and the rebar effect must be considered. It could be the subject of the next step of this research by changing geometric conditions.

This study presents in six sections. The first section is the introduction. The second section explains how the glue layer replaces with springs and the way their stiffness determine. The third section introduces the EFG method and the scheme of applying the concept of the adhesive element in the formulation. The fourth section notes the details of the numerical example, properties of the beam and materials, node placement procedure, and reference experiment. In the fifth part, numerical results are compared with the experimental study of Kim and her colleagues, and in the sixth section, the conclusion is presented.

## 2 Approximating the adhesive layer with a set of springs

The main proposed idea is to replace adhesive layer behavior with a set of nonlinear horizontal and vertical springs (Fig. 2(a)). The nature of replaced springs is depicted in Fig. 2(b). The stiffness of these springs is assumed constant

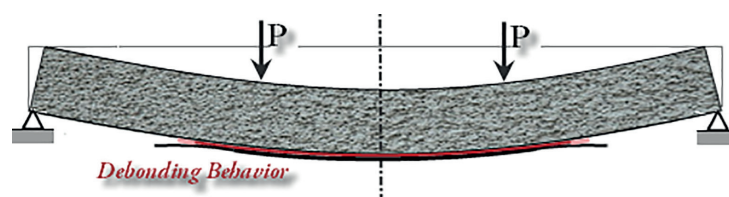


Fig. 1 Debonding at the end of the FRP plate [21]

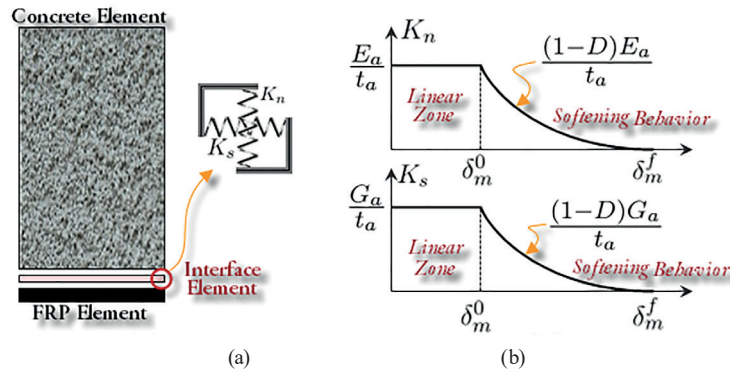


Fig. 2 Adhesive layer; (a) Modeling adhesive layer with spring, (b) Nonlinear spring stiffness diagram

during the elastic behavior region. In the following, after glue reaches the damage initiation stage, it enters the non-linear phase and will become decremental, and finally, after debonding, it comes to zero.

In Fig. 2  $t_a$  is the adhesive thickness,  $G_a$  and  $E_a$  are shear modulus and elasticity modulus,  $D$  is the damage parameter and has different values,  $K_n$  and  $K_s$  are vertical and horizontal spring stiffness.  $\delta_m^0$  and  $\delta_m^f$  are relative displacements of springs in the damage threshold and the separation moment, respectively.

## 2.1 Determination of springs stiffness

### 2.1.1 Linear behavior

The behavior of equivalent springs is linear and reversible as far as the damage has not been initiated in the adhesive layer. In these conditions, stiffness is a function of the elastic modulus of glue and its thickness. The stiffness values for horizontal and vertical springs are as below:

$$t_{n(x)} = K_n \Delta U y_{(x)} = K_n (u_y^2 - u_y^1), \quad (1)$$

$$K_n = \frac{t_{n(x)}}{\Delta U y_{(x)}} = \frac{t_{n(x)}}{\frac{\Delta U y_{(x)}}{t_a}} \times \frac{1}{t_a} = \frac{t_{n(x)}}{\epsilon_{n(x)} t_a} \times \frac{1}{t_a} = E_a \times \frac{1}{t_a} = \frac{E_a}{t_a}, \quad (2)$$

$$t_{s(x)} = K_s \Delta U x_{(x)} = K_s (u_x^2 - u_x^1), \quad (3)$$

$$K_s = \frac{t_{s(x)}}{\Delta U x_{(x)}} = \frac{t_{s(x)}}{\frac{\Delta U x_{(x)}}{t_a}} \times \frac{1}{t_a} = \frac{t_{s(x)}}{\gamma_{s(x)} t_a} \times \frac{1}{t_a} = G_a \times \frac{1}{t_a} = \frac{G_a}{t_a}. \quad (4)$$

$u_y^1$  is vertical displacement at the joint boundary of adhesive and concrete,  $u_y^2$  is vertical displacement at the joint boundary of adhesive and FRP.  $u_x^1$  and  $u_x^2$  are horizontal displacement at the top and bottom of the joint boundary, respectively.  $t_n(x)$  and  $t_s(x)$  are normal and shear stress in the adhesive layer. As the applied load increases, deformations rise, and the glue reaches its yield strength. So, the softening phase starts.

### 2.1.2 Damage initiation and evolution

Damage evolution shows that spring stiffness is decreasing. From a physical point of view, the adhesion property in the glue represents connection persistence and its structural strength. When the adhesive thickness is thin, using a cohesion element with softening behavior is an acceptable assumption for describing glue strength and surfaces debonding [28]. Needleman expresses if the resistance between two surfaces is weaker than the resistance between adhered components and the thickness of the adhesive is thin, the adhesive models show a better performance [28].

Based on the adhesive model, a traction-separation diagram is considered for the glue (Fig. 3). According to this diagram, sticky behavior is assumed linear with the  $K$  parameter as penalty stiffness.  $K$  is a mechanical property of the glue and determined via experiment. Softening starts (point A) after the formation of a small increase in the adhesive thickness ( $\delta_m^0$ ). By increasing the load, its stiffness reduces up to the point that relative separation forms ( $\delta_m^f$ ). At this moment (point B), debonding happens [29, 30].

A scaler parameter,  $D$ , is used to consider stiffness variations. It indicates the level of damage at different points of the glue. Its value is assumed to be zero before damage initiates ( $D = 0$ ). After on,  $D$  starts to rise gradually up to 1 (complete adhesive separation). During the damage

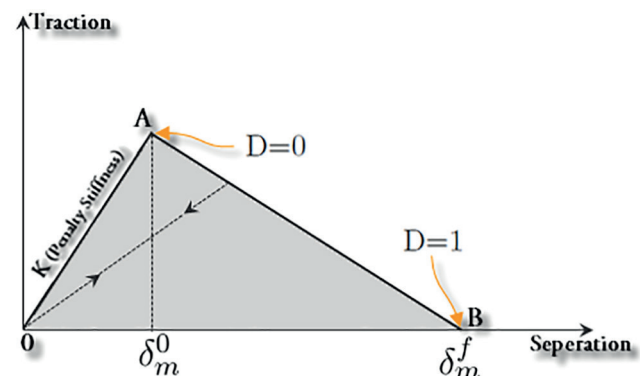


Fig. 3 Traction-separation diagram in adhesive layer [28, 29]

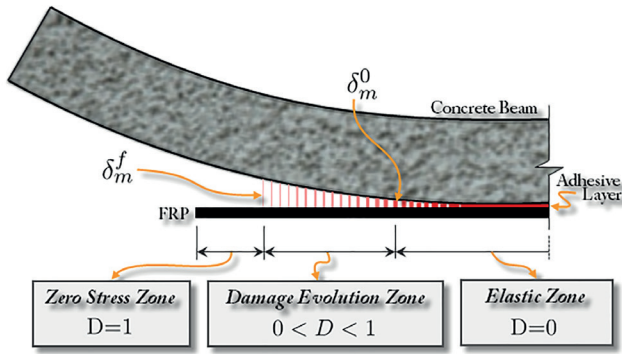


Fig. 4 Separation manner in glue in three regions [31, 32]

progression phase, the springs stiffness decrease by  $(1-D)$  factor.  $D$  will be described in Section 2.2. According to Fig. 4, these phases can be divided into three parts; linear region (elastic), nonlinear zone (damage evolution), and separation district (zero-stress).  $\delta_m^0$  and  $\delta_m^f$  relative displacements of springs in the damage threshold and the separation moment, respectively [31, 32]. By considering three behavior phases in spring, its stiffness value is defined as below:

$$K_s = \begin{cases} \frac{G_a}{t_a} & \delta_m^{\max} < \delta_m^0 \\ \frac{(1-D)G_a}{t_a} & \delta_m^0 \leq \delta_m^{\max} < \delta_m^f \\ 0 & \delta_m^f \leq \delta_m^{\max} \end{cases}, \quad (5)$$

$$K_n = \begin{cases} \frac{E_a}{t_a} & \delta_m^{\max} < \delta_n^0 \\ \frac{(1-D)E_a}{t_a} + \frac{DE_a}{t_a} \frac{-\delta_n}{-\delta_n} & \delta_n^0 \leq \delta_m^{\max} < \delta_n^f \\ \frac{E_a}{t_a} \frac{-\delta_n}{-\delta_n} & \delta_n^f \leq \delta_m^{\max} \end{cases}. \quad (6)$$

Parameter  $\delta_n$  is the relative vertical displacement, and  $\delta_m^{\max}$  is the maximum effective relative separation experienced by a point of the glue during loading. There is one exception to Eq. (6).  $\langle \dots \rangle$  is the Macaulay bracket. It means that if the displacement of the bottom node is less the corresponding upper node,  $\delta_n$  becomes lower than zero ( $\delta_n < 0$ ), which means that the adhesive layer is under compression. So, separation can not occur in the vertical direction. In the softening phase,  $K_s$  and  $K_n$  have a common parameter,  $D$ . So, their values are interdependent. In this study,  $K_n$  becomes equal to  $\frac{E_a}{t_a}$  and the stiffness of the vertical spring will be constant.  $K_s$  is assumed constant during the elastic behavior region. In the following,

after glue reaches the damage initiation stage, it enters the nonlinear phase and will become decremental, and finally, in the debonding phase, it comes to zero. After calculating spring stiffness and determination of relative horizontal displacement at the common interface ( $\delta_s$ ), shear stress in glue can be determined by the following Eq. (7):

$$t_s = K_s \delta_s. \quad (7)$$

The relative displacement values in the adhesive layer have two components. One of them is relative horizontal displacement ( $\delta_s$ ) used to determine shear stress in the glue, and the other component is relative vertical displacement, ( $\delta_n$ ) which is used to determine normal stress. The values of  $\delta_s$  and  $\delta_n$  are obtained as follows:

$$\delta_s = u_x^{2(\text{Bottom node})} - u_x^{1(\text{Top node})}, \quad (8)$$

$$\delta_n = u_y^{2(\text{Bottom node})} - u_y^{1(\text{Top node})}. \quad (9)$$

So, traction vector  $\mathbf{t}$  in a two-dimensional state is expressed as follows [33]:

$$\begin{bmatrix} \mathbf{t}_s \\ \mathbf{t}_n \end{bmatrix} = \begin{pmatrix} K_s & 0 \\ 0 & K_n \end{pmatrix} \begin{bmatrix} \delta_s \\ \delta_n \end{bmatrix}. \quad (10)$$

The damage process initiates when stress or separation at the contact surface satisfies the damage initiation criterion. Various criteria, such as maximum stress or maximum relative surface separation, have been proposed. Since both shear and vertical slips occur, considering the simultaneous influence of these two slips can be a more realistic criterion. Fig. 5 represents the traction-separation diagram of adhesive under the simultaneous effect of normal and shear stresses. As is seen in Fig. 5, one of the two criteria of quadratic separation or quadratic stress can be considered [34].

Since, in the EFG method, the interface displacement can be achieved easily, the Quadratic Separation Method is chosen to apply. According to this model, damage in the cohesive element initiates when the sum of the squares of the relative separations in Eq. (11) becomes equal to one.

$$\left( \frac{\langle \delta_n \rangle}{\delta_n^0} \right)^2 + \left( \frac{\delta_s}{\delta_s^0} \right)^2 = 1 \quad (11)$$

According to Fig. 5,  $\delta_n^0$  is the damage initiation deformation when only normal stress exists, and  $\delta_s^0$  is for when only shear stress exists. Macaulay bracket is presented by the following relation (Eq. (12)) [35, 36]:

$$\langle \delta_n \rangle = \begin{cases} 0 & \delta_n \leq 0 \\ \delta_n & \delta_n > 0 \end{cases}. \quad (12)$$

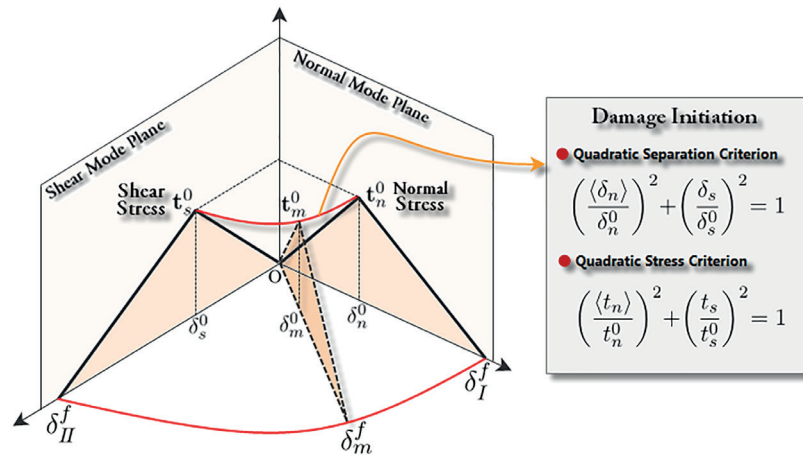


Fig. 5 Combined diagram of traction-separation under the simultaneous effect of normal and shear stresses [34]

In the next part, the numerical criterion of damage evolution parameter,  $D$  is presented.

### 2.2 Damage evolution parameter

The damage parameter,  $D$  equal to zero means corruption has not initiated. In the case of , the damage is in the growth phase, but separation has not occurred yet. Finally, if  $D = 1$  then, separation has occurred. According to the definitions, the value of parameter  $D$  will be [35, 36]:

$$D = \frac{\delta_m^f (\delta_m^{\max} - \delta_m^0)}{\delta_m^{\max} (\delta_m^f - \delta_m^0)} \quad (13)$$

As is shown in Fig. 5,  $\delta_m^0$  is the relative displacement during damage initiation and  $\delta_m^f$  is the relative displacement at the instant of full separation. The numerical value of these parameters is obtained from the below relation:

$$\delta_m^0 = \begin{cases} \delta_n^0 \delta_s^0 \sqrt{\frac{1+m^2}{(\delta_s^0)^2 + m^2 (\delta_n^0)^2}} & \delta_n > 0 \\ \delta_s^0 & \delta_n \leq 0 \end{cases}, \quad (14)$$

$$\delta_n^0 = \frac{\sigma_c}{K}, \quad \delta_s^0 = \frac{\tau_c}{K}, \quad m = \frac{\delta_s}{\delta_n}$$

$$\delta_m^f = \begin{cases} \frac{2}{K \delta_m^0} \left[ G_{IC} + (G_{IIC} - G_{IC}) \left( \frac{m^2}{1+m^2} \right)^\eta \right] & \delta_n > 0 \\ \frac{2G_{IIC}}{\tau_s^0} & \delta_n \leq 0 \end{cases}. \quad (15)$$

The value of  $\tau_c$  and  $\sigma_c$  are the maximum shear stress and maximum tensile stress tolerable by adhesive in the linear range, and the parameter  $K$  is penalty stiffness. The

value of  $G_{IC}$  is the strain energy due to normal stress of the glue and  $G_{IIC}$  is strain energy due to shear stress of the glue. All these parameters, along with coefficient  $\eta$ , are the mechanical properties of the glue and have been determined by experiments [36, 37]. The parameter  $\delta_m^{\max}$  is the maximum effective relative displacement experienced by the adhesive during its loading.  $\delta_m$  is the effective relative separation parameter, which is defined as follows:

$$\delta_m = \sqrt{\langle \delta_n \rangle^2 + \delta_s^2}. \quad (16)$$

It can be seen from Eq. (16) that in order to determine the damage evolution criterion, the combined effect of horizontal and vertical displacements is considered simultaneously.

### 3 Element Free Galerkin method

Element Free Galerkin method (EFG) is one of the numerical methods based on the minimum squares method. Adequate accuracy can be achieved by choosing nodal points, suitable weight functions with considering the boundary conditions. In this approach, there is no need for establishing a connection between all nodes; interactions between surrounding nodes are enough [26, 38]. The main unknown is the value of nodal displacements, which can be obtained utilizing springs and the cohesive element concept in the EFG method structure. After measuring nodal displacements, the magnitude of the debonding load, shear stress values in the adhesive, concurrently with the tensile strain in the FRP plate, can be obtained.

#### 3.1 Generating shape functions using MLS method

Based on the MLS method, the unknown function  $u(x)$  is approximated with function  $u^h(x)$  as below:

$$u^h(x) = \sum_{j=1}^m p_j(x) a_j(x) = p^T(x) a(x), \quad (17)$$

where  $p(x)$  is a vector of polynomial basis function, and  $a(x)$  is a vector of unknown coefficients depend on  $x$  position.  $m$  is the number of basis function terms. Linear and second-order functions are ordinarily basis functions in the MLS method.  $a_j(x)$  coefficients are obtained from minimizing residual weighed square function. This function is expressed as:

$$J = \sum_{l=1}^n W(x-x_l) [p^T(x_l) a(x) - u_l]^2, \quad (18)$$

where  $u_l$  is the nodal parameter for field variable, and  $n$  is the number of nodes located inside the coverage domain neighboring  $x$ .  $W(x-x_l)$  is the weight function. In this study, a widely used fourth-order spline weight function is utilized.  $u^h(x)$  is determined by minimizing  $J$  and solving the resulted linear equations as Eq. (19):

$$u^h(x) = \sum_{l=1}^n \phi_l(x) u_l = \Phi(x) U_s. \quad (19)$$

In Eq. (19),  $U_s$  is the quantity vector of variables in nodes inside the domain and  $\Phi(x)$  is the matrix of shape functions, which is defined as shown below:

$$\Phi(x) = [\phi_1(x) \phi_2(x) \dots \phi_n(x)] = p^T(x) A^{-1}(x) B(x). \quad (20)$$

$A$  is the weight function matrix, and  $B$  is the values of the basic functions in the nodes. The stiffness matrices calculation needs first-order derivatives of the variables. So, derivatives of the shape functions must be calculated [26, 38]. In the next subsection, the resulted EFG equations and the way for the implementation of springs modeling are presented.

### 3.2 Extraction of discrete equations

Overall potential energy for the beam and the FRP plate will be:

$$L = U + W = \sum_{k=1,2} \left( \frac{1}{2} \int_{\Omega} \varepsilon^T D_k \varepsilon d\Omega_k \right) + \int_{\Gamma_s} \frac{1}{2} K_n (u_y^{(2)} - u_y^{(1)})^2 d\Gamma + \int_{\Gamma_s} \frac{1}{2} K_s (u_x^{(2)} - u_x^{(1)})^2 d\Gamma, \quad (21) - \int_{\Omega} u^T b d\Omega - \int_{\Gamma_t} u^T \bar{t} d\Gamma - \sum_{i=1}^{n_{CF}} F_i u_i$$

where numbers 1 and 2 are assigned to the concrete beam and FRP plate, respectively.  $\varepsilon$  is the strain vector,  $D_k$  is the properties matrix of materials,  $\Omega$  is the domain, and  $\Gamma_s$  is the adhesive boundary.  $u_x^{(k)}$  and  $u_y^{(k)}$  are the horizontal

and vertical displacements of the material on the interface.  $u$  is the displacement vector. The volume force represented with  $b$ .  $\bar{t}$  is the traction vector in boundaries, and  $F_i$  is the  $i$ th concentrated load.  $u_i$  is the displacement vector in  $i$ th load location, and  $n_{CF}$  is the number of applied forces. Second and third terms on the right side of the Eq. (21) belong to the influence of springs with cohesive structure. Stiffness values of ( $K_s$ ) and ( $K_n$ ) have already presented in Eqs. (5) and (6).

A remarkable point about Eq. (21) is MLS shape functions have not the Kronecker delta function properties ( $\phi_l(x_j) \neq \delta_{lj}$ ), and for, boundary conditions of the problem ( $\Gamma_u$ ) are applied through penalty function.

The example considered in this research is symmetric, so half of the structure is modeled. The total potential energy introduced in Eq. (21) is modified by applying boundary conditions and penalty functions. Then the principle of minimum potential energy can be applied and is obtained as Eqs. (22) and (23):

$$\tilde{L} = L + \int_{\Gamma_u} \frac{1}{2} (\tilde{u} - \bar{u})^T \alpha (\tilde{u} - \bar{u}) d\Gamma \Rightarrow \delta \tilde{L} = 0, \quad (22)$$

$$\begin{aligned} &\rightarrow \sum_{k=1,2} \left( \int_{\Omega} \delta \varepsilon^T D_k \varepsilon d\Omega_k \right) \\ &+ \int_{\Gamma_s} \delta (u^{(2)} - u^{(1)})^T D_a (u^{(2)} - u^{(1)}) d\Gamma \\ &- \int_{\Omega} \delta u^T b d\Omega - \int_{\Gamma_t} \delta u^T \bar{t} d\Gamma - \sum_{i=1}^{n_{CF}} F_i \delta u_i \\ &+ \int_{\Gamma_u} \delta (\tilde{u} - \bar{u})^T \alpha (\tilde{u} - \bar{u}) d\Gamma = 0 \end{aligned} \quad (23)$$

In Eqs (22) and (23),  $u^{(k)}$  is the displacement vector of the  $k$ th material on the adhesive boundary  $\Gamma_s$ , which must be approximated on the domain  $\Omega_k$ .  $\bar{u}$  and  $\tilde{u}$  are the values of displacement or rotation in boundary ( $\Gamma_u$ ). Also,  $\alpha$  is the diagonal matrix containing penalty coefficients.  $D_a$  is the stiffness matrix of the glue defined as Eq. (24):

$$D_a = \begin{bmatrix} K_s & 0 \\ 0 & K_n \end{bmatrix}. \quad (24)$$

The displacement field is approximated in terms of nodal parameters by introducing the MLS shape functions in Eq. (23). The final discrete equations system is obtained as Eq. (25):

$$[K_{LJ} + K_{LJ}^A + \tilde{K}_{LJ}] U = F. \quad (25)$$

In this equation,  $U$  is the vector of nodal parameters related to beam displacement.  $K_{LJ}$  is the influence of the structural stiffness in the global stiffness matrix. It will

achieve so by applying the MLS approximation on the terms which, represent the internal virtual work of both beam and the plate.

$$K_{IJ} = \sum_{k=1,2} \left[ \int_{\Omega_k} R_I^T D_k R_J d\Omega_k \right], \quad (26)$$

where:

$$R_I = \begin{bmatrix} \frac{\partial \phi_I}{\partial x} & 0 \\ 0 & \frac{\partial \phi_I}{\partial y} \\ \frac{\partial \phi_I}{\partial y} & \frac{\partial \phi_I}{\partial x} \end{bmatrix}. \quad (27)$$

Matrix  $K_{IJ}^A$  in Eq. (25) belongs to springs with a cohesive structure and is determined using the following Eq. (28):

$$K_{IJ}^A = \sum_{k=1,2} \int_{\Gamma_s} [\phi_I^1 - \phi_I^2]^T D_a [\phi_J^1 - \phi_J^2] d\Gamma. \quad (28)$$

Matrix  $\tilde{K}_{IJ}$  in Eq. (25) is resulted from applying geometrical constraints with corresponding penalty coefficients  $\alpha$ .

$$\tilde{K}_{IJ} = \int_{\Gamma_u} (L_b \phi_I)^T \alpha (L_b \phi_J) d\Gamma \quad (29)$$

Finally, components of F are calculated as follows Eq. (30):

$$F = \int_{\Omega} \phi_I b d\Omega + \int_{\Gamma_f} \phi_I \bar{t} d\Gamma + \sum_{i=1}^{n_{oc}} (\phi_I)_i F_i. \quad (30)$$

Equation (25) will be solved by incremental applying of the external load. In each step of loading using spring modeling, the first node with the damage index,  $D$ , so close or equal to one is investigated. The amount of load correspond to this step is identified as the debonding load. Afterward, the shear stress of the glue and the tensile strain of the plate are determined through Eq. (7) using node displacement in the interface of FRP and the glue. In the next section, the whole process are applied and the properties of the example are presented.

#### 4 Numerical example

This section explains a numerical example of the method. Also, includes properties of the assumed beam and materials, the node placement procedure, as well as the results of Kim et al. [39, 40].

#### 4.1 Beam properties

Fig. 6 shows the sample used in this research. The lengths of beam and FRP sheet are 2800 mm and 1800 mm, respectively. The beam has 250 mm height and is subjected under two concentrated loads, which will be applied incrementally.

#### 4.2 Materials properties

The properties for the concrete beam and the FRP plate are given in Table 1. The specifications of the adhesive layer are listed in Table 2.

#### 4.3 Node placement in the EFG method

As mentioned before, only half of the beam is considered for analysis due to symmetry. The numbers of selected nodes in the concrete beam are 80 along the longitudinal direction and 10 along with the height. The numbers of nodes along the longitudinal and thickness of the FRP plate are 60 and 3, respectively. Fig. 7, illustrates the placement of the nodes in the left half of the example. The closeness of nodes in the FRP is due to the low thickness.

#### 4.4 Experiment results

The properties of the beam and FRP plate in the mentioned example are similar to the properties of the experiment in Kim et al. [39, 40] to compare the results. They used a potentiometer in the mid-span of the beam to measure vertical

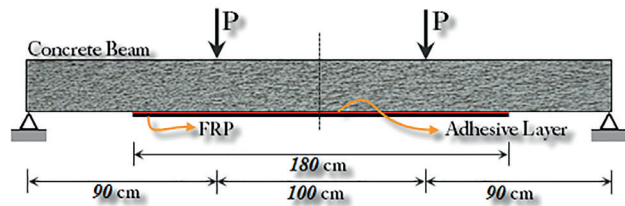


Fig. 6 The simply supported beam with FRP plate and two concentrated loads applied to the beam

Table 1 Geometric and mechanical properties of concrete and FRP [39,40]

Concrete beam properties				
Length(mm)	Height(mm)	$f_c$ (MPa)	$E_c$ (MPa)	$\nu_c$
2800	250	30	23700	0.15
Mechanical properties of FRP plate				
Length(mm)	Thickness(mm)	$f_{pu}$ (MPa)	$E_{FRP}$ (MPa)	$\nu_{FRP}$
1800	1	4500	245000	0.3

Table 2 Mechanical properties of the adhesive layer [36, 39, 40]

Thickness(mm)	$\tau_n^0$ (MPa)	$\tau_s^0$ (MPa)	$K$ (N/m <sup>3</sup> )	GIC(J/m <sup>2</sup> )	GIIC(J/m <sup>2</sup> )	$\eta$
0.2	80	80	$10^{14}$	1740	2890	2.3

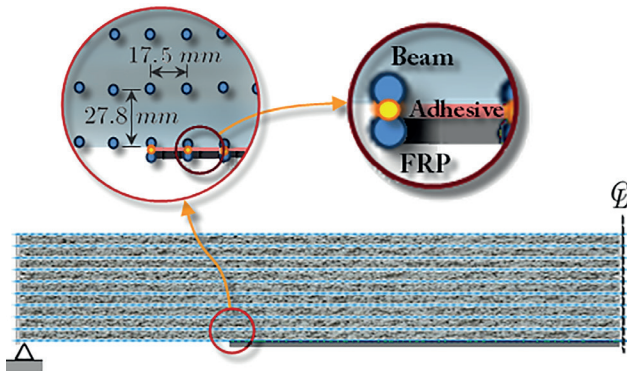


Fig. 7 Node placement in beam and FRP plate

displacement and some strain gauges along the FRP to measure the deformation of the plate. The load increase and continues until the first debonding occurs in the glue. The first separation point happened on the side edge of the FRP [39, 40].

The parameters determined are the load corresponding to the moment of the first separation, adhesive shear stress, and the amount of tensile strain along the length of the FRP plate. Table 3 presents the results of the experiment of Kim et al. [39, 40].

In the following section, the numerical results of EFG are compared with the experimental results of Kim et al. [39, 40].

### 5 Numerical results and comparison

In this section, the results obtained by the EFG method are compared with the results of the experimental tests of Kim et al. [39, 40]. The first subsection is dedicated to the comparison of load-deflection at the moment of adhesive separation. The second and third subsections compare the glue shear stresses and FRP plate tensile strains with experimental results, respectively.

#### 5.1 Deflection in mid span due to external load

As can be seen in Fig. 8, the horizontal axis of the diagram depicts mid-span deflection, and the vertical axis

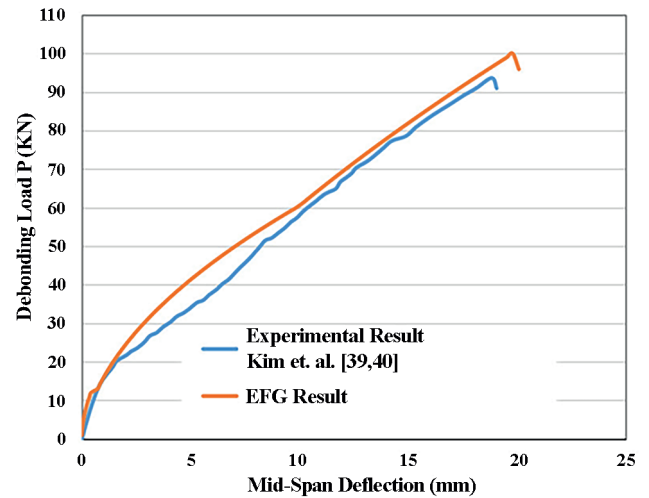


Fig. 8 Load-mid-span vertical deflection at the moment of first debonding

represents the applied load (P). The value of debonding load is given as 100.4 kN from EFG numerical analysis and 93.8 kN in the reference paper [39, 40]. At this moment, the mid-span deflection is determined by the EFG method at about 19.7 mm and reported at 18.8 mm from experimental tests by Kim et al. [39, 40]. In the diagram of the EFG results, a tiny step is observed around the 12 kN load range. This step is due to damage initiation and softening phenomena in the glue.

#### 5.2 Adhesive shear stress results

The results of adhesive shear stress at the moment of separation are shown in Fig. 9. The horizontal and vertical axes represent FRP plate length and adhesive shear stress, respectively. The highest shear stress in the glue occurs close to the edge of the FRP plate. This behavior can be observed in the EFG results and, to some extent, in the experimental results of Kim et al. [39, 40]. In EFG results, the stress has some decremental trend in the plate edge, which is due to adhesive softening phenomena. In both diagrams, adhesive shear stress decreases in the middle of

Table 3 The output of the experimental result in three sections [39, 40]

Experimental results 2 and 3			Experimental results 1	
Distance from FRP plate edge X (mm)	Shear stress in adhesive (MPa)	Tensile strain in FRP plate (Micron)	Loading value until first separation (KN)	Vertical deflection of the beam (mm)
65	2.4	0	0	0
204	1.79	0	26.8	3.1
339	1.8	300	38.8	6.2
481	1.35	332	52.3	8.7
613	1.33	1015	65.1	11.7
742	1.43	1750	84.2	16.1
860	1.05	2337	97.5	20.9

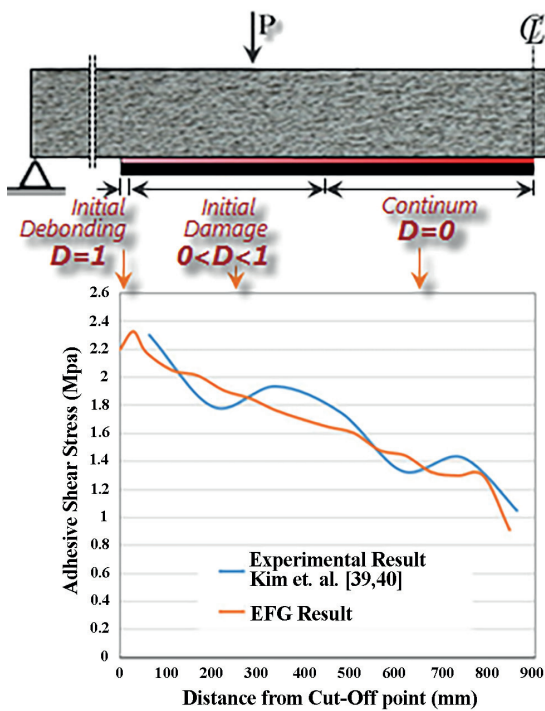


Fig. 9 Maximum shear stress in the adhesive during load debonding

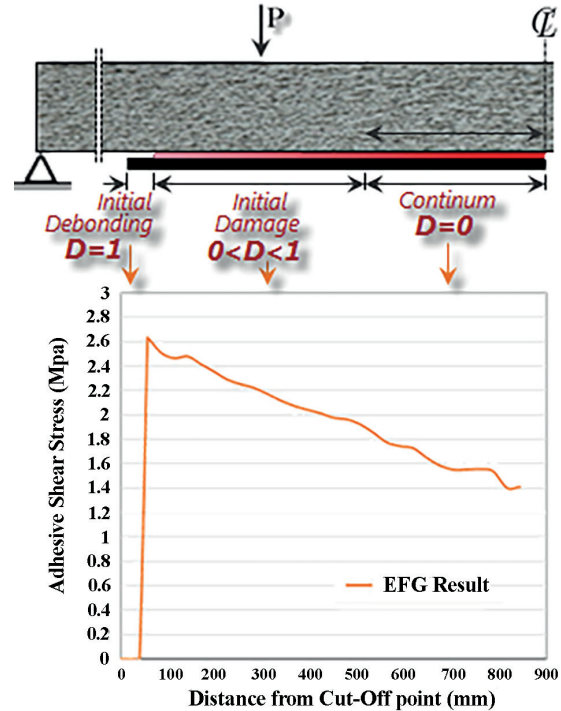


Fig. 10 Shear stress in the adhesive as the load increases and passes the debonding load

the span because of the small shear deformations in this area. By comparing the curves in Fig. 9, it can be seen that the result of the EFG method is smoother and more uniform than the experimental results.

In the following the applied load increases from 100.4 KN to 110 KN. It has been found that more length of the adhesive is separated (Fig. 10). In other words, by increasing the load, debonding increases, and the equivalent stiffness of springs, and consequently, shear stresses in these regions become zero. The location of the maximum shear stress moves slightly toward the mid-span and is placed close to the new separated point. Since no experiment has been performed in the reference paper of Kim et al. [39, 40], only the results of the EFG method are presented.

### 5.3 FRP plate tensile strain results at the moment of debonding

Fig. 11 shows the results of the tensile strain in the FRP. The horizontal axis of the diagram displays the length of the plate, and the vertical axis shows the strain. Since the bending moment in the middle of the beam is high, the maximum tensile strain of the FRP occurs in this area. This issue appeared in both the EFG results and in the experiment of Kim et al [39, 40]. By nearing to the end of the plate, the tensile strain reduces. At the end part of the FRP where debonding occurs, tensile strain approximates to zero. In other words, as the plate separates, no force is

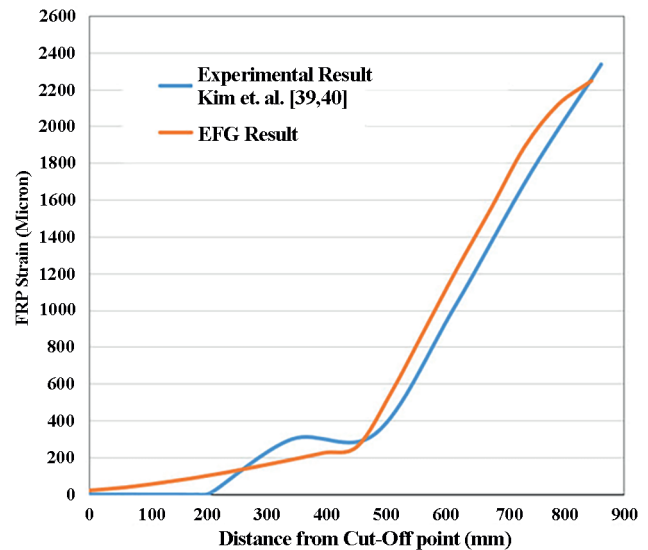


Fig. 11 FRP plate tensile strain during debonding

transferred to the plate, and the resulted strain becomes zero. By comparing the results, it can be seen that the EFG method output is smoother than the other.

## 6 Conclusions

The goal of this research is to provide an alternative numerical method to laboratory experiments. It will reduce the immense costs of the practical tests. A simple concrete beam with an FRP plate was used under two concentrated loads.

For the numerical solution to this problem and to take into account the nonlinear behavior of the glue, a spring simulation was employed using the cohesive element failure concept. Properties and influences of the cohesive elements have been introduced into the EFG method formulation as the stiffness matrix of the replaced springs. By incremental applying of the load, the values of the debonding load, adhesive shear stresses, and FRP tensile strains were calculated. The results of the numerical EFG method were compared with the experimental results of Kim et al [39, 40].

Results show that the idea of representing the behavior of the adhesive layer with a set of horizontal and vertical springs works very well. With this replacement, it is easy

to determine the amount of deformation and the conditions of the adhesive layer. Also, results show that with continuous springs simulation and the cohesive element failure model for evaluating the glue layer phenomena, the EFG numerical method can bring reasonable accuracy to the results. Hence, hard practical experiments with immense costs can be avoided.

As mentioned before, in this study, a beam with a specific geometry and dimensions was used. In future studies, this modeling method will be applied to other examples with different geometric conditions to find the capacity of the proposed idea.

## Reference

- [1] Hosny, A., Sayed-Ahmed, E. Y., Abdelrahman, A. A., Alhlaby, N. A. "Strengthening precast prestressed hollow core slabs to resist negative moments using CFRP strips: an experimental investigation and a critical review of CSA 806-02", *Canadian Journal of Civil Engineering*, 33(8), pp. 955–967, 2006.  
<https://doi.org/10.1139/106-040>
- [2] Ritchie, P. A., Thomas, D. A., Lu, L.-W., Connelly, M. G. "External reinforcement of concrete beams using fiber reinforced plastics", *ACI Structural Journal*, 88(4), pp. 490–500, 1991.  
<https://doi.org/10.14359/2723>
- [3] Saadatmanesh, H., Ehsani, M. R. "RC Beams strengthened with GFRP plates. I: Experimental study", *Journal of Structural Engineering*, 117(11), pp. 3417–3433, 1991.  
[https://doi.org/10.1061/\(ASCE\)0733-9445\(1991\)117:11\(3417\)](https://doi.org/10.1061/(ASCE)0733-9445(1991)117:11(3417))
- [4] Napoli, A., Realfonzo, R. "Reinforced concrete beams strengthened with SRP/SRG systems: experimental investigation", *Construction and Building Materials*, 93, pp. 654–677, 2015.  
<https://doi.org/10.1016/j.conbuildmat.2015.06.027>
- [5] Huang, L., Yan, B., Yan, L., Xu, Q., Tan, H., Kasal, B. "Reinforced concrete beams strengthened with externally bonded natural flax FRP plates", *Composites Part B*, 91, pp. 569–578, 2016.  
<https://doi.org/10.1016/j.compositesb.2016.02.014>
- [6] Moradi, E., Naderpour, H., Kheyroddin, A. "An experimental approach for shear strengthening of RC beams using a proposed technique by embedded through-section FRP sheets", *Composite Structures*, 238, Article number: 111988, 2020.  
<https://doi.org/10.1016/j.compstruct.2020.111988>
- [7] Shadravan, B., Tehrani, F. M. "A Review of direct shear testing configurations for bond between fiber-reinforced polymer sheets on concrete and masonry substrates", *Periodica Polytechnica Civil Engineering*, 61(4), pp. 740–751, 2017.  
<https://doi.org/10.3311/PPci.9090>
- [8] Szabó, Z. K., Balázs, G. L. "Near surface mounted FRP reinforcement for strengthening of concrete structures", *Periodica Polytechnica Civil Engineering*, 51(1), pp. 33–38, 2007.  
<https://doi.org/10.3311/pp.ci.2007-1.05>
- [9] Ibrahim, S. K., Movahedi Rad, M. "Numerical Plastic Analysis of Non-Prismatic Reinforced Concrete Beams Strengthened by Carbon Fiber Reinforced Polymers", In: *Proceedings of the 2020 session of the 13th fib International PhD Symposium in Civil Engineering*, Paris, France, 2020, pp. 208–215. [online] Available at: [https://phdsymp2020.sciencesconf.org/data/pages/Proceedings\\_phdsymp\\_2021.pdf](https://phdsymp2020.sciencesconf.org/data/pages/Proceedings_phdsymp_2021.pdf)
- [10] Chellapandian, M., Parakash, S. S., Sharma, A. "Experimental and finite element studies on the flexural behavior of reinforced concrete elements strengthened with hybrid FRP technique", *Composite Structures*, 208, pp. 466–478, 2019.  
<https://doi.org/10.1016/j.compstruct.2018.10.028>
- [11] Heffernan, P. J., Erki, M. A. "Equivalent capacity and efficiency of reinforced concrete beams strengthened with carbon fiber reinforced plastic sheets", *Canadian Journal of Civil Engineering*, 23(1), pp. 21–29, 1996.  
<https://doi.org/10.1139/196-003>
- [12] De Lorenzis, L. "Some recent results and open issues on interface modeling in civil engineering structures", *Materials and Structures*, 45, pp. 477–503, 2012.  
<https://doi.org/10.1617/s11527-012-9830-5>
- [13] Lu, X. Z., Teng, J. G., Ye, L. P., Jiang, J. J. "Bond-slip models for FRP sheets/plates bonded to concrete", *Engineering Structures* 27(6), pp. 920–937, 2007.  
<https://doi.org/10.1016/j.engstruct.2005.01.014>
- [14] Maalej, M., Bian, Y. "Interfacial shear stress concentration in FRP-strengthened beams", *Composite Structures*, 54(4), pp. 417–426, 2001.  
[https://doi.org/10.1016/S0263-8223\(01\)00078-2](https://doi.org/10.1016/S0263-8223(01)00078-2)
- [15] Arduini, M., Nanni, A. "Behavior of Precracked RC Beams Strengthened with Carbon FRP Sheets", *Journal of Composites for Construction*, 1(2), pp. 63–70, 1997.  
[https://doi.org/10.1061/\(ASCE\)1090-0268\(1997\)1:2\(63\)](https://doi.org/10.1061/(ASCE)1090-0268(1997)1:2(63))
- [16] Carpinteri, A., Cornetti, P., Pugno, N. "Edge debonding in FRP strengthened beams: stress versus energy failure criteria", *Engineering Structures*, 31(10), pp. 2436–2447, 2009.  
<https://doi.org/10.1016/j.engstruct.2009.05.015>

- [17] Smith, S. T., Teng, J. G. "FRP-strengthened RC beams. I. review of debonding strength model", *Engineering Structures*, 24(4), pp. 385–395, 2002.  
[https://doi.org/10.1016/S0141-0296\(01\)00105-5](https://doi.org/10.1016/S0141-0296(01)00105-5)
- [18] Smith, S. T., Teng, J. G. "FRP-strengthened RC beams. II. assessment of debonding strength models", *Engineering Structures* 24(4), pp. 397–417, 2002.  
[https://doi.org/10.1016/S0141-0296\(01\)00106-7](https://doi.org/10.1016/S0141-0296(01)00106-7)
- [19] ACI Committee 440 "ACI 440.2 R-02 Guide for the design and construction of externally bonded FRP systems for strengthening concrete structures", American Concrete Institute, Farmington Hills, MI, USA, 2005.
- [20] CSA "CSA S806-02 Design and construction of building components with fiber-reinforced polymers", Canadian Standards Association, Toronto, ON, Canada, 2002.
- [21] Sayed-Ahmed, E. Y., Bakay, R., Shrive, N. G. "Bond strength of FRP laminates to concrete: State of the art review", *Electronic Journal of Structural Engineering*, 9, pp. 45–61, 2009.
- [22] Teng, J. G., Chen, J. F., Smith, S. T., Lam, L. "FRP Strengthened RC Structures", John Wiley, New York, NY, USA, 2002.
- [23] Barenblatt, G. I. "The mathematical theory of equilibrium cracks in brittle fracture", *Advances in Applied Mechanics*, 7(1), pp. 55–129, 1962.  
[https://doi.org/10.1016/S0065-2156\(08\)70121-2](https://doi.org/10.1016/S0065-2156(08)70121-2)
- [24] Dugdale, D. S. "Yielding of steel sheets containing slits", *Journal of the Mechanics and Physics of Solids*, 8(2), pp. 100–104, 1960.  
[https://doi.org/10.1016/0022-5096\(60\)90013-2](https://doi.org/10.1016/0022-5096(60)90013-2)
- [25] Alfano, G., Sacco, E. "Combining interface damage and friction in a cohesive zone model", *International Journal for Numerical Methods in Engineering*, 68(5), pp. 542–582, 2006.  
<https://doi.org/10.1002/nme.1728>
- [26] Belytschko, T., Lu, Y. Y., Gu, L. "Element-free Galerkin methods", *International Journal for Numerical Methods in Engineering*, 37(2), pp. 229–256, 1994.  
<https://doi.org/10.1002/nme.1620370205>
- [27] Li, S., Liu, W. K. "Meshfree and particle methods and their applications", *Applied Mechanics Reviews*, 55(1), pp. 1–34, 2002.  
<https://doi.org/10.1115/1.1431547>
- [28] Needleman, A. "A continuum model for void nucleation by inclusion debonding", *Advances in Applied Mechanics*, 54(3), pp. 525–531, 1987.  
<https://doi.org/10.1115/1.3173064>
- [29] Hadjazi, K., Sereir, Z., Amziane, S. "Cohesive zone model for the prediction of interfacial shear stresses in a composite plate RC beam with an intermediate flexural crack", *Composite Structures*, 94(12), pp. 3574–3582, 2012.  
<https://doi.org/10.1016/j.compstruct.2012.05.027>
- [30] Wu, Z., Yin, J. "Fracturing behaviors of FRP-strengthened concrete structure", *Engineering Fracture Mechanics*, 70(10), pp. 1339–1355, 2003.  
[https://doi.org/10.1016/S0013-7944\(02\)00100-5](https://doi.org/10.1016/S0013-7944(02)00100-5)
- [31] Barbero, E. J. "Delaminations", In: Barbero, E. J. (ed.) *Finite Element Analysis of Composite Materials using Abaqus™*, CRC Press, Boca Raton, FL, USA, 2013, pp. 353–375.  
<https://doi.org/10.1201/b14788>
- [32] Brandão, M. F., Cimini, C. A. "Cohesive models for damage evolution in adhesive joints using finite element", presented at 38th Iberian Latin American Congress on Computational Methods in Engineering, Florianópolis, Brazil, Nov. 5–8, 2017.  
<https://doi.org/10.20906/CPS/CILAMCE2017-0887>
- [33] ABAQUS "ABAQUS Theory Manual, (Version 6.7)", [computer program] (online) Available at: <http://130.149.89.49:2080/v6.7/books/stm/default.htm>
- [34] Saeid, A. A., Donaldson, S. L. "Experimental and finite element investigations of damage resistance in biomimetic composite sandwich t-joints", *Materials*, 9(7), Article number: 510, 2016.  
<https://doi.org/10.3390/ma9070510>
- [35] Camanho, P. P., Dávila, C. D. "Mixed-Mode Decohesion Finite Elements for the Simulation of Delamination in Composite Materials", NASA, Hampton, VI, USA, Rep. NASA/TM-2002-211737, 2002.
- [36] Naghipour, P., Bartsch, M., Voggenreiter, H. "Simulation and experimental validation of mixed mode delamination in multidirectional CF/PEEK laminates under fatigue loading", *International Journal of Solids and Structures*, 48(6), pp. 1070–1081, 2011.  
<https://doi.org/10.1016/j.ijsolstr.2010.12.012>
- [37] Benzeggagh, M. L., Kenane, M. "Measurement of mixed-mode delamination fracture toughness of unidirectional glass/epoxy composites with mixed-mode apparatus", *Composites Science and Technology*, 56(4), pp. 439–449, 1996.  
[https://doi.org/10.1016/0266-3538\(96\)00005-X](https://doi.org/10.1016/0266-3538(96)00005-X)
- [38] Liu, G. R. "Meshfree Methods: Moving Beyond the Finite Element Method", *Applied Mechanics Reviews*, 56(2), pp. B17–B18, 2009.  
<https://doi.org/10.1115/1.1553432>
- [39] Kim, N., Kim, Y.-H., Kim, H. S. "Experimental study for evaluating structural behavior of RC beams strengthened by different width of FRP layers", *International Journal of Engineering and Technology*, 5(6), pp. 662–665, 2013.  
<https://doi.org/10.7763/IJET.2013.V5.637>
- [40] Kim, N., Shin, Y. S., Choi, E., Kim, H. S. "Relationships between interfacial shear stresses and moment capacities of RC beams strengthened with various types of FRP sheets", *Construction and Building Materials*, 93, pp. 1170–1179, 2015.  
<https://doi.org/10.1016/j.conbuildmat.2015.05.007>